THICKNESS MEASUREMENT OF A NONMAGNETIC METALLIC PLATE USING HARMONIC EDDY CURRENT EXCITATION AND A GMR SENSOR

A. Lopes Ribeiro [1,2], *Helena G.Ramos*[1,2], *J.Couto Arez*[1,2]

[1] Instituto de Telecomunicações, Lisboa, Portugal, arturlr@ist.utl.pt
[2] Instituto Superior Técnico, Universidade Técnica de Lisboa, Portugal

Abstract: This paper describes the implementation of a device that measures the thickness of metallic plates. A pancake coil for magnetic field sinusoidal excitation is used and detection is performed with a bridge giant magneto-resistor sensor. The paper uses the theory of the linear transformer to explain the liftoff effect with a special attention to the point of intersection phenomenon.

Keywords: eddy currents, giant magneto-resistor sensor, liftoff, linear transformer theory.

1. INTRODUCTION

The eddy current method (ECM) is currently applied in nondestructive evaluation of metallic materials [1-3]. It is widely used to detect, localize and characterize defects inside those materials. It is especially useful when the objects under test are only accessed from one external surface. However, this method is only usable on metallic media to detect defects at small depths.

This paper describes the application of the ECM to measure the thickness of metallic non-ferromagnetic plates. The method may be applied in metallic foils production or to detect material loss due to corrosion [4].

Other authors have tackled this problem, using different approaches that mainly differ by the excitation currents in use. Some authors prefer single or multi-frequency harmonic excitation and others prefer pulsed excitation [5-7] to take advantage from the richer signal frequency content.

The reason to avoid a single frequency is due to the liftoff problem, which results from the difficulty in maintaining a constant gap between the probe and the material. Thus, correlating the signals obtained for different frequencies, it is possible to infer about the liftoff gap [8].

In this paper we use single frequency excitation and a giant magneto-resistor sensor (GMR). The GMR allows the excitation with frequencies much lower than those used with inductive detection. Allying greater penetration depths, obtained with lower frequencies, to the increased sensibility of the GMRs it is possible to construct an apparatus that can use low frequency excitation. The liftoff phenomenon will be studied and solved using the linear transformer theory [9].

In the next section the experimental setup is presented, describing the electric circuitries for excitation and detection. In section 3 we present the linear transformer theory applied to the coil-plate system. Finally, in section 4 we discuss the experimental results.

2. THE EXPERIMENTAL SETUP

The experimental setup is depicted in Fig. 1, including a pancake coil with 300 turns, external radius $R_e = 15$ mm, internal radius $R_i = 5.5$ mm and height $H = 8$ mm. A giant magneto-resistor is inserted along the coil axis, with the sensing direction perpendicular to the plate. A sinusoidal voltage generator drives a transadmittance amplifier that injects the excitation current in the pancake coil. In this way a constant primary excitation field is guaranteed independently of liftoff variations and consequent impedance coil changes. The sensor voltage output is amplified by an instrumentation amplifier and acquired by a NI-USB-6251 16-bit acquisition board.

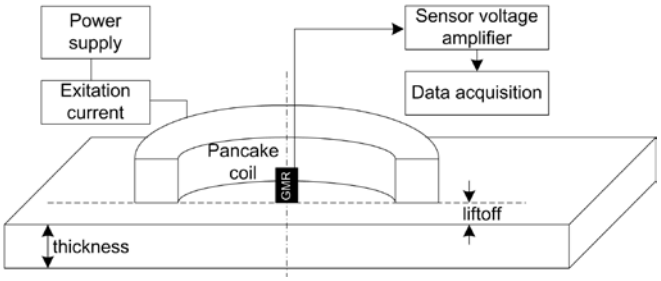

Fig. 1. Experimental setup.

2.1. GMR sensor and electric circuitry

Figure 2 depicts the internal configuration of the giant magneto-resistor sensor AA002-02 produced by Non-Volatile Electronics.

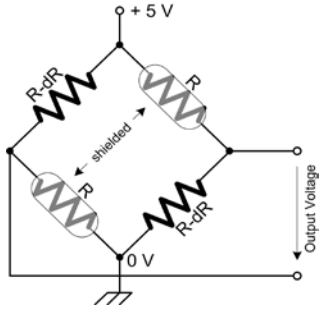

Fig. 2. Giant magneto-resistor bridge sensor.

Four giant magneto-resistors are connected in a bridge configuration, with two of them magnetically shielded.

Figure 3 represents the output GMR sensor voltage as a function of the magnetic flux density. The typical V-shaped characteristic determines the necessity of a DC bias. Being the measurement direction along the coil axis, the bias is obtained by using a DC offset in the excitation current. In the linear regions the AA002-02 sensor presents a sensitivity around 4 mV/V-Oe. This sensitivity corresponds in S.I. units to the characteristic in Fig.3, for a DC supply voltage of 5 V.

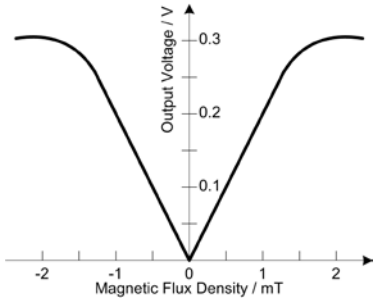

Fig. 3. AA002-02 GMR sensor output characteristic for a supply voltage of 5 V.

Figure 4 depicts the transadmittance amplifier in use. The L2722 operational amplifier is indicated for power amplification, particularly for driving inductive loads, allowing a maximum output current of 1 A. R_1 is used as a sampling resistor allowing the measurement of the excitation current.

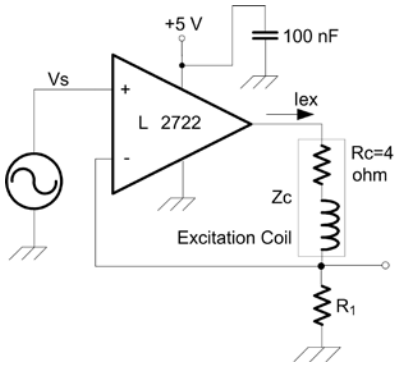

Fig. 4 Transadmittance excitation current generator.

Figure 5 shows the scheme in use to amplify the sensor output voltage. The time-constant RC of the high-pass filters between the sensor and the INA118 amplifier is set to attenuate the low frequency noise below f =150 Hz, and R_G sets the amplification gain.

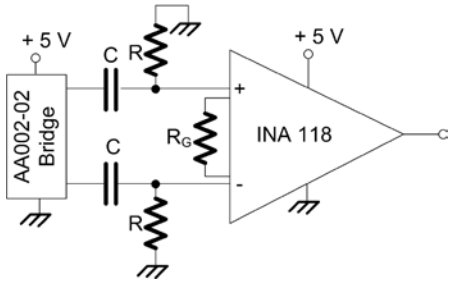

Fig. 5. INA output signal amplifier.

3. TRANSFORMER THEORY

In his section the theory of the linear transformer will be revisited to understand if the plate under inspection in our setup, presented in Fig.1, can be represented as the short-circuited secondary of a linear transformer.

Let us assume that we have two circuits magnetically coupled. The reference directions of voltages and currents are depicted in Fig. 6.

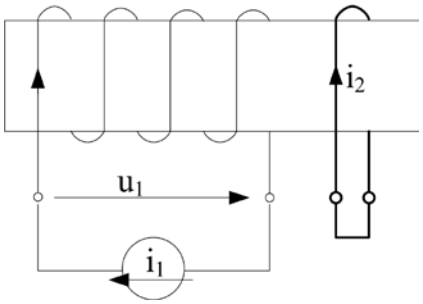

Fig. 6. Representation of the reference directions of currents and voltages in the equivalent transformer.

The electrical parameters of the transformer windings are as follows: r_1 is the primary resistance and r_2 is the resistance of the short-circuited secondary; L_{11} and L_{22} are the self-inductance coefficients of the primary and secondary respectively, and L_M is the mutual inductance coefficient between windings, defined as a positive quantity, due to the relative reference directions defined for the currents i_1 and i_2. In the sinusoidal regime, the equations that relate voltages and currents in the transformer with the short-circuited secondary are

$$\begin{cases} \bar{U}_1 = (r_1 + j\omega L_{11})\bar{I}_1 + j\omega L_M \bar{I}_2 \\ 0 = j\omega L_M \bar{I}_1 + (r_2 + j\omega L_{22})\bar{I}_2 \end{cases} \quad (1)$$

The equations (1) may be represented in terms of an equivalent circuit, as depicted in Fig. 7, including an ideal transformer, with the primary to secondary number of turns ratio given by ν, and the non-idealities represented by a T-shaped circuit. The relation between the currents is

$$i'_2 = -i_2/\nu \quad , \quad i_1 = i_{10} - i'_2 = i_1 + i_2/\nu \, . \quad (2)$$

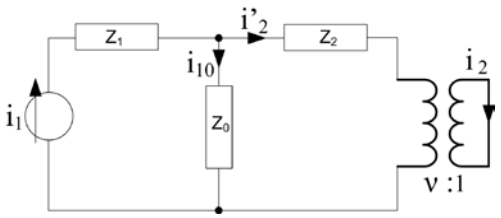

Fig. 7. Topology of the transformer equivalent circuit.

The current i_{10} is the magnetization current referenced to the primary. Being the ratio $\nu = n_1 / n_2$, then

$$n_1 i_{1\,0} = n_1 i_1 + n_2 i_2 \, . \quad (3)$$

Thus, i_{10}, alone in the primary, presents a magneto-motive force equal to the current i_1 in the primary and i_2 together in the secondary. The circuit in Fig. 7 is specified in Fig. 8, with the impedances given by

$$\begin{cases} \bar{Z}_1 = r_1 + j\omega\lambda_{11} = r_1 + j\omega(L_{11} - \nu L_M) \\ \bar{Z}_0 = j\omega l_{11} = j\omega\nu L_M \\ \bar{Z}_2 = r'_2 + j\omega\lambda'_{22} = \nu^2 r_2 + j\omega\nu^2(L_{22} - L_M/\nu) \end{cases} \quad (4)$$

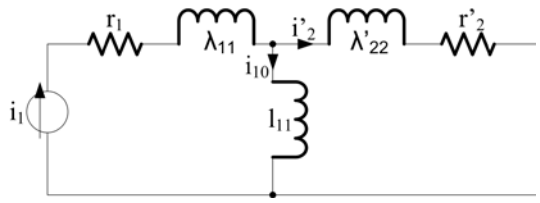

Fig. 8. The transformer equivalent circuit referred to the primary (excitation) winding.

The parameter $\lambda_{11} = L_{11} - \nu L_M$ represents the leakage flux linked to primary, and $\lambda_{22} = L_{22} - L_M/\nu$ represents the leakage flux linked to the secondary. The parameter $l_{11} = \nu L_M$ is the induction coefficient relative to the main flux linked simultaneously to both windings. The parameters with primes represent the quantities in the secondary as seen on the primary.

It is important to refer that the parameter ν, when unknown, can be postulated, with the restriction that in this way, it is only possible to determine the external quantities, which are the voltages and the currents measurable on the transformer terminals. However, if ν is available, the internal quantities such as the leakage fluxes and the main linkage flux can be obtained from the equivalent circuit model.

3.1 The magnetic coupling factor

It is well known that the measurements obtained in eddy current experiments, strongly depend on the distance between the excitation coil and the metallic material under test. We shall model the distance variation, known in the non-destructive testing applications as the liftoff effect, by changing the magnetic coupling factor k between the primary and secondary of the model transformer

$$k = \frac{L_M}{\sqrt{L_{11}L_{22}}}. \quad (5)$$

We shall assume that the distance variation between the excitation coil and the plate, in the real experimental setup, is small in order that the parameters r_2 and L_{22} connected to the secondary (testing plate) remain unchanged.

3.2 Forcing a primary sinusoidal excitation

We will now determine the consequences of applying a sinusoidal excitation $i_1(t) = I_1\cos(\omega t)$ to the primary winding. The phasor of i_{10} is determined as

$$\bar{I}_{10} = \frac{r'_2 + j\omega\lambda'_{22}}{r'_2 + j\omega(l_{11} + \lambda'_{22})}\bar{I}_1. \quad (6)$$

and taking into account the magnetic coupling dependence, according to (5), the secondary flux leakage parameter must be changed to

$$\lambda'_{22} = \nu^2(L_{22} - L_M/\nu) = \nu^2 L_{22} - \nu k\sqrt{L_{11}L_{22}}. \quad (7)$$

With this relation we can represent $\bar{I}_{10}$ as

$$\bar{I}_{10} = \frac{r'_2 + j\omega\nu^2 L_{22} - j\omega\nu k\sqrt{L_{11}L_{22}}}{r'_2 + j\omega\nu^2 L_{22}}\bar{I}_1 = \left(1 - \frac{j\omega\nu k\sqrt{L_{11}L_{22}}}{r'_2 + j\omega\nu^2 L_{22}}\right)\bar{I}_1 \quad (8)$$

This equation shows that the variation of the coupling factor k results in a variation of $\bar{I}_{10}$ equal to

$$\Delta\bar{I}_{10} = -\frac{j\omega\nu\sqrt{L_{11}L_{22}}}{r'_2 + j\omega\nu^2 L_{22}}\bar{I}_1\Delta k. \quad (9)$$

The current in the secondary is almost in opposition to the primary current. Thus, when the coupling factor increases, the current $\bar{I}_{10}$ decreases. The opposition would be exactly verified if the secondary resistance r_2 was null. Figure 9 represents the variations described by (9).

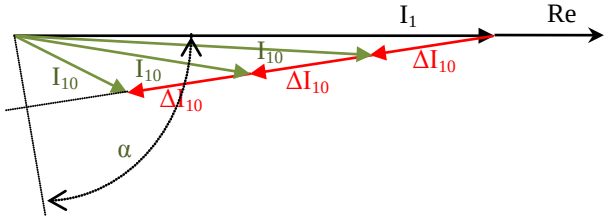

Fig. 9. Phasors of the magnetization current variations.

The phase of $\Delta\bar{I}_{10}$ relative to the primary current $\bar{I}_1$ is independent of the coupling factor k,

$$\arg\{\Delta\bar{I}_{10}\} = -\frac{\pi}{2} - \arctan\left\{\frac{\omega\nu^2 L_{22}}{r'_2}\right\} = -\frac{\pi}{2} - \alpha \quad (10)$$

according to the assumption that the parameters relative to the secondary (the plate) don't change with k. Thus, there will be one instant of time $t_0 = \alpha/\omega$, designated liftoff point of intersection (LOI) for which the instantaneous value $i_{10}(t_0)$ is independent of k.

In Fig. 10 the magnetization currents obtained for five different values of the magnetic coupling factor are displayed (k = 0.75; 0.8; 0.85; 0.9; 0.95). All the curves present points of intersection, that occur periodically, in a instant of time that can be anticipated using (10).

The importance of this result is based on the fact that a similar result was obtained experimentally, which confirms the rightness of the transformer approach. The experimental access to the magnetization current is done by measuring the output voltage of the GMR magnetometer. The placement of this sensor in the axis of the excitation coil and near the plate is such that it measures the magnetization effect of the

excitation current and the resultant eddy currents in the plate. Thus, the GMR senses indirectly the magnetization current $i_{10}(t)$.

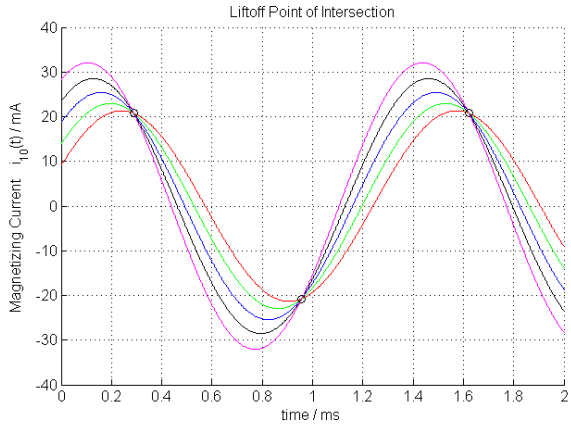

Fig. 10. Instantaneous values of the magnetization current for five different values of the coupling factor showing the LOI.

3.2 The transformer input impedance

Another way to verify if the transformer model accurately represents the real situation is by measuring the input impedance. The short-circuit impedance is easily obtained from equation (1),

$$\overline{Z}_{sc} = (r_1 + j\omega L_{11}) + \frac{\omega^2 L_M^2}{r_2 + j\omega L_{22}}. \qquad (11)$$

In (11) the first term represents the impedance of the excitation coil and the second represents the influence of the secondary (the plate) on the primary. Our hypothesis rely on the constancy of the secondary parameters r_2 and L_{22}. If in (11) we represent the mutual inductance L_M in terms of the magnetic coupling factor we obtain,

$$\overline{Z}_{sc} = \overline{Z}_{11} + \overline{Z}_{12} = (r_1 + j\omega L_{11}) + \frac{\omega^2 k^2 L_{11} L_{22}}{r_2 + j\omega L_{22}} \qquad (12)$$

Let us now look at the experimental data to determine the real effectiveness of the results presented in Fig. 10 and in equation (12).

3.3 The transformer model and the experimental data

Figures 11 and 12 show some of the experimental data collected from the magnetic field measurements taken from the GMR sensor for two different plates. As stated before these measurements indirectly represent the magnetization current $i_{10}(t)$.

The collected data show that it is possible to determine the plate thickness from the determination of the time point of intersection, assuming that the material conductivity remains the same. It was possible to show that the excitation current intercepts the curves depicted in Fig.s 11 and 12, at the same point. This result was previewed from the transformer theory, at the phasor diagram in Fig. 9. Being confirmed that a point of intersection exists, it is possible to take a profit from that knowledge: being the plate thickness related to the curves amplitude, we must take the measurements exactly at the interception time.

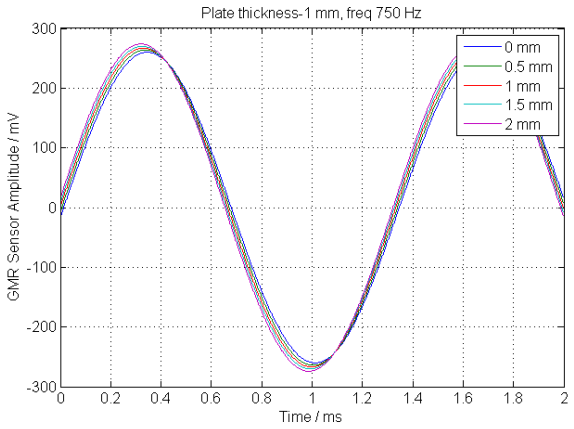

Fig. 11. Instantaneous values of the GMR voltage with excitation @ 750 Hz, plate thickness=1 mm and 5 different gaps.

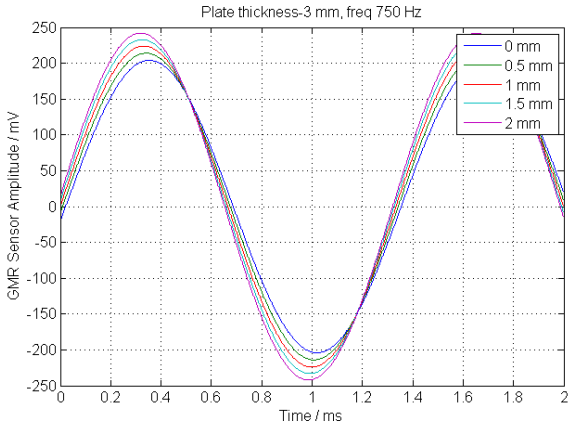

Fig. 12. Instantaneous values of the GMR voltage with excitation @ 750 Hz, plate thickness=3 mm and 5 different gaps.

The short-circuit impedance in (12) may be further explored. The term of influence of the secondary over the primary may be represented as

$$\overline{Z}_{12} = \Delta\overline{Z} = \frac{\omega^2 k^2 L_{11} L_{22}}{r_2^2 + \omega^2 L_{22}^2}(r_2 - j\omega L_{22}) \qquad (13)$$

Figure 13 represents the transformer impedance $\overline{Z}_1$ increments measured as a function of the liftoff distance.

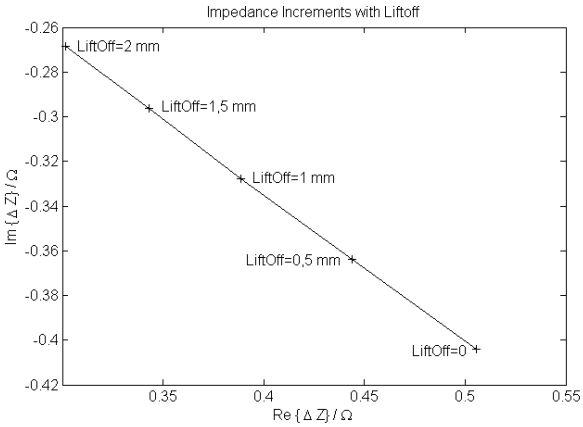

Fig. 12. Excitation coil impedance @ 750 Hz, plate thickness=1 mm and 5 different liftoff gaps.

The type of variations shows proportionality to the complex conjugate of secondary impedance when the magnetic coupling increases, or equivalently when the liftoff gap decreases.

4. RESULTS AND CONCLUSION

The constructed apparatus was used with aluminum plates of type AL3105-H12, with the electric conductivity $\sigma = 26.18$ MS/m . Five material thicknesses from one to four millimeters were obtained by stacking a different number of plates.

Figure 13 represents the amplitude of the voltages obtained for an excitation current $I_{ex} = 100$ mA and frequency $f_{ex} = 750$ Hz . At this frequency, and for the material conductivity given above, the standard penetration depth is $\delta = 4.24$ mm .

As expected, the sensor output voltage decreases for greater thicknesses. The eddy currents inside the aluminum are almost in opposition with the primary coil excitation current, and the magnetic field along the coil axis is reduced, especially close to the aluminum, where the GMR is placed. It is also noted that the voltage amplitude tends to a constant value for increased thicknesses. This fact shows the difficulty in the detection of the field created by the deeper and weaker levels of the eddy currents. Figure 13 also depicts the error bound assumed for the GMR voltage measurement. The uncertainty in the measurement of the GMR output voltage is depicted as 1 mV. This value results from the resulting uncertainty in the measurement of sine waveforms using a sine fitting algorithm.

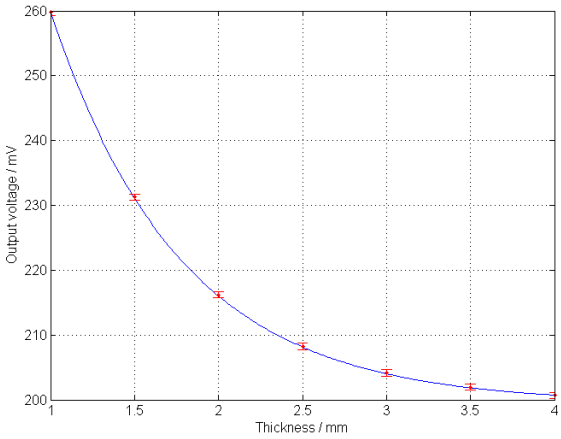

Fig. 13. Excitation coil impedance @ 750 Hz, plate thickness=1 mm and 5 different liftoff gaps.

In Fig. 14 the same data represented in the previous figure is now displayed with the thickness as a function of the detected amplitude voltage. An exponential curve fits in the experimental data with minor errors in the GMR relative to the experimental data.

However, the discrepancies between the fitted curve and the experimental data are now more evident when we try to access the larger thicknesses. This result is due to the smaller sensitivity of the GMR output to the eddy currents in the lower plate layers. Some further study and experimental work is needed to improve that sensitivity.

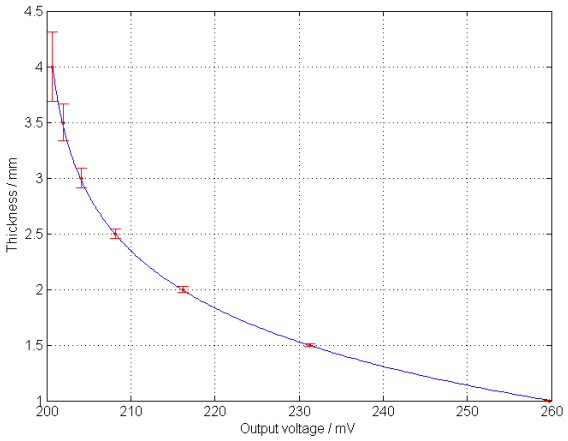

Fig. 14. Output voltage versus material thickness.

ACKNOWLEDGMENT

The Instituto de Telecomunicações - Projects OMeGA and KeMANDE, supported this work. This support is gratefully acknowledged.

REFERENCES

[1] A.L. Ribeiro, H.G. Ramos, O. Postolache, "A Simple Forward Direct Problem Solver for Eddy Current Non-destructive Inspection of Aluminum Plates Using Uniform Field Probes", Measurement 2011. http://dx.doi.org/10.1016/j.measurement.2011.03.029

[2] O. Postolache, H. Geirinhas Ramos, A. Lopes Ribeiro, "Detection and characterization of defects using GMR probes and artificial neural networks", Computer Standards & Interfaces, vol.33, pp.191-200, 2011.

[3] A. Lopes Ribeiro, H. Geirinhas Ramos, "Inductive Probe for Flaw Detection in non-Magnetic Metallic Plates Using Eddy Currents", Proc. I2MTC-IEEE International Instrumentation and Measurement Technology Conference, Victoria, Canada, pp.1447-1453, 12-15 May, 2008.

[4] C.S. Angani, et al., "Differential pulsed eddy current sensor for the detection of wall thinning in an insulated stainless steel pipe", Journal of App. Physics, vol.107,Issue 9, Proceedings of the 11th Joint MMM-Intermag Conference, Washington DC 2010.

[5] C. Mandache, J.H.V. Lefebvre, "Transient and harmonic eddy currents: Liftoff point of intersection", NDT&E International, vol.39, 2006, pp.57-60.

[6] Y-K. Shin, D-M. Choi, Y-J. Kim, S-S. Lee, "Signal characteristics of differential-pulsed eddy current sensors in the evaluation of plate thickness", NDT&E International, vol.42, 2009, pp.215-221.

[7] J. Kral, R. Smid, H.M. Geirinhas Ramos, A. Lopes Ribeiro, "Thickness Measurement Using Transient Eddy

Current Techniques", International Instrumentation and Measurement Technology Conference, pp.138-143, Binjiang, Hangzhou, China, May 2011.

[8] A. Lopes Ribeiro, F. Alegria, O. Postolache, H. G. Ramos, "Liftoff Correction Based on the Spatial Spectral Behavior of Eddy-Current Images", IEEE Trans. on Instrumentation and Measurement, vol.59, n.5, pp.1362-1367, May 2010.

[9] T. Le Bihan, "Study on the transformer equivalent circuit of eddy current nondestructive evaluation", NDT&E International, vol.36, 2003, pp.297-302.